
Exact Diffusion Inversion via Bi-directional Integration Approximation

Guoqiang Zhang

University of Technology Sydney (UTS)
guoqiang.zhang@uts.edu.au

J.P. Lewis

Nvidia
jpl@nvidia.com

W. Bastiaan Kleijn

Victoria University of Wellington
bastiaan.kleijn@vuw.ac.nz

Abstract

Recently, different methods have been proposed to address the inconsistency issue of DDIM inversion to enable image editing, such as EDICT [36] and Null-text inversion [22]. However, the above methods introduce considerable computational overhead. In this paper, we propose a new technique, named *bi-directional integration approximation* (BDIA), to perform exact diffusion inversion with negligible computational overhead. Suppose we would like to estimate the next diffusion state z_{i-1} at timestep t_i with the historical information (i, z_i) and $(i+1, z_{i+1})$. We first obtain the estimated Gaussian noise $\hat{\epsilon}(z_i, i)$, and then apply the DDIM update procedure twice for approximating the ODE integration over the next time-slot $[t_i, t_{i-1}]$ in the forward manner and the previous time-slot $[t_i, t_{i+1}]$ in the backward manner. The DDIM step for the previous time-slot is used to refine the integration approximation made earlier when computing z_i . One nice property with BDIA-DDIM is that the update expression for z_{i-1} is a linear combination of $(z_{i+1}, z_i, \hat{\epsilon}(z_i, i))$. This allows for exact backward computation of z_{i+1} given (z_i, z_{i-1}) , thus leading to exact diffusion inversion. Interestingly, the update expression for z_{i-1} is in fact time-symmetric in that switching the timestep t_{i-1} and t_{i+1} produces the inverse update expression for z_{i+1} in terms of (z_i, z_{i-1}) . Experiments on both image reconstruction and image editing were conducted, confirming our statement.

BDIA can also be applied to improve the performance of other ODE solvers in addition to DDIM. In our work, it is found that applying BDIA to the EDM sampling procedure produces slightly better FID score over CIFAR10.

1 Introduction

As one type of generative models, diffusion probabilistic models (DPMs) have made significant progress in recent years. The pioneering work [31] applied non-equilibrium statistical physics to estimating probabilistic data distributions. In doing so, a Markov forward diffusion process is constructed by systematically inserting additive noise into a data sample until the data distribution is almost destroyed. The data distribution is then gradually restored by a reverse diffusion process starting from a simple parametric distribution. The main advantage of DPM over classic tractable models (e.g., HMMs, GMMs, see [4]) is that DPM can accurately model both the high and low likelihood regions of the data distribution by estimating a sequence of progressively less noise-perturbed data distributions. In comparison to generative adversarial networks (GANs) [9; 1; 10; 29],

DPMs exhibit more stable training dynamics by avoiding adversarial learning, as well as showing better sample diversity.

Following the work of [31], various learning and/or sampling strategies have been proposed to improve the performance of DPMs, which include, for example, denoising diffusion probabilistic models (DDPMs) [11], denoising diffusion implicit models (DDIMs) [32], improved DDIMs [23; 6], latent diffusion models (LDMs)[25], score matching with Langevin dynamics (SMLD) [34; 33; 35], analytic-DPMs [3; 2], optimized denoising schedules [18; 5; 19], guided diffusion strategies [24; 16], and classifier-free guided diffusion [12]. It is worth noting that DDIM can be interpreted as a first-order ODE solver. As an extension of DDIM, various high-order ODE solvers have been proposed, such as EDM [15], DEIS [40], PNDM [20], DPM-Solvers [21], and IIA-EDM and IIA-DDIM [39].

In recent years, image-editing via diffusion models has attracted increasing attention in both academia and industry. One important operation for editing a real image is to first perform forward process on the image to obtain the final noise representation and then perform a backward process with embedded editing to generate the desired image [26; 28]. DDIM inversion has been widely used to perform the above forward and backward processes [30]. A major issue with DDIM inversion is that the intermediate diffusion states in the forward and backward processes may be inconsistent due to the inherent approximations (see Subsection 3.1). This issue becomes significant when utilizing classifier-free guided technique in text-to-image editing [30]. The newly generated images are often perceptually far away from the original ones, which is undesirable for image-editing.

Recently, two methods have been proposed to address the inconsistency issue of DDIM inversion. Specifically, the work of [22] proposed a technique named *null-text inversion* to push the diffusion states of the backward process to be optimally close to those of the forward process via iterative optimization. The null-text inputs to the score neural network are treated as free variables in the optimization procedure. In [36], the authors proposed the EDICT technique to enforce exact DDIM inversion. Their basic idea is to introduce an auxiliary diffusion state and then perform alternating updates on the primal and auxiliary diffusion states, which is inspired by the flow generative framework [17; 7; 8]. One drawback of EDICT is that the number of neural functional evaluations (NFEs) has to be doubled in comparison to DDIM inversion (See Subsection 3.2). Another related line of research work is DDPM inversion (see [13]).

In this paper, we propose a new technique to enforce exact DDIM inversion with negligible computational overhead, reducing the number of NFEs required in EDICT by half. Suppose we are in a position to estimate the next diffusion state z_{i-1} at timestep t_i by utilizing the two most recent states z_i and z_{i+1} . With the estimated Gaussian noise $\hat{\epsilon}(z_i, i)$, we perform the DDIM update procedure twice for approximating the ODE integration over the next time-slot $[t_i, t_{i-1}]$ in the forward manner and the previous time-slot $[t_i, t_{i+1}]$ in the backward manner. The DDIM for the previous time-slot is employed to refine the integration approximation made earlier when computing z_i . As a result, the expression for z_{i-1} becomes a linear combination of $(z_{i+1}, z_i, \hat{\epsilon}(z_i, i))$, and naturally facilitates exact diffusion inversion. We refer to the above technique as *bi-directional integration approximation (BDIA)*. We emphasize that the obtained update expression for z_{i-1} under BDIA-DDIM is time-symmetric in that switching the timestep t_{i-1} and t_{i+1} inverts the diffusion directions (see Section 4 for a discussion on relevant literature). Experiments demonstrate that BDIA-DDIM produces satisfactory results on both image reconstruction and image editing. We have also applied BDIA to EDM, and found that the image qualities are also improved slightly.

2 Preliminary

Forward and reverse diffusion processes: Suppose the data sample $\mathbf{x} \in \mathbb{R}^d$ follows a data distribution $p_{data}(\mathbf{x})$ with a bounded variance. A forward diffusion process progressively adds Gaussian noise to the data samples \mathbf{x} to obtain z_t as t increases from 0 until T . The conditional distribution of z_t given \mathbf{x} can be represented as

$$q_{t|0}(z_t|\mathbf{x}) = \mathcal{N}(z_t|\alpha_t\mathbf{x}, \sigma_t^2\mathbf{I}) \quad z_t = \alpha_t\mathbf{x} + \sigma_t\epsilon, \quad (1)$$

where α_t and σ_t are assumed to be differentiable functions of t with bounded derivatives. We use $q(z_t; \alpha_t, \sigma_t)$ to denote the marginal distribution of z_t . The samples of the distribution $q(z_T; \alpha_T, \sigma_T)$ should be practically indistinguishable from pure Gaussian noise if $\sigma_T \gg \alpha_T$.

The reverse process of a diffusion model firstly draws a sample \mathbf{z}_T from $\mathcal{N}(\mathbf{0}, \sigma_T^2 \mathbf{I})$, and then progressively denoises it to obtain a sequence of diffusion states $\{\mathbf{z}_{t_i} \sim p(\mathbf{z}; \alpha_{t_i}, \sigma_{t_i})\}_{i=0}^N$, where we use the notation $p(\cdot)$ to indicate that reverse sample distribution might not be identical to the forward distribution $q(\cdot)$ because of practical approximations. It is expected that the final sample \mathbf{z}_{t_0} is roughly distributed according to $p_{data}(\mathbf{x})$, i.e., $p_{data}(\mathbf{x}) \approx p(\mathbf{z}_{t_0}; \alpha_{t_0}, \sigma_{t_0})$ where $t_0 = 0$.

ODE formulation: In [35], Song et al. present a so-called *probability flow* ODE which shares the same marginal distributions as \mathbf{z}_t in (1). Specifically, with the formulation (1) for a forward diffusion process, its reverse ODE form can be represented as

$$d\mathbf{z} = \underbrace{\left[f(t)\mathbf{z}_t - \frac{1}{2}g^2(t)\nabla_{\mathbf{z}} \log q(\mathbf{z}_t; \alpha_t, \sigma_t) \right]}_{d(\mathbf{z}_t, t)} dt, \quad (2)$$

where $d(\mathbf{z}_t, t)$ denotes the gradient vector at time t , and the two functions $f(t)$ and $g(t)$ are represented in terms of (α_t, σ_t) as

$$f(t) = \frac{d \log \alpha_t}{dt}, \quad g^2(t) = \frac{d\sigma_t^2}{dt} - 2 \frac{d \log \alpha_t}{dt} \sigma_t^2. \quad (3)$$

$\nabla_{\mathbf{z}} \log q(\mathbf{z}; \alpha_t, \sigma_t)$ in (2) is the score function [14] pointing towards higher density of data samples at the given noise level (α_t, σ_t) . One nice property of the score function is that it does not depend on the generally intractable normalization constant of the underlying density function $q(\mathbf{z}; \alpha_t, \sigma_t)$.

As t increases, the probability flow ODE (2) continuously reduces the noise level of the data samples in the reverse process. In the ideal scenario where no approximations are introduced in (2), the sample distribution $p(\mathbf{z}; \alpha_t, \sigma_t)$ approaches $p_{data}(\mathbf{x})$ as t goes from T to 0. As a result, the sampling process of a diffusion model boils down to solving the ODE form (2), where randomness is only introduced in the initial sample at time T . This has opened up the research opportunity of exploiting different ODE solvers in diffusion-based sampling processes.

Denoising score matching: To be able to utilize (2) for sampling, one needs to specify a particular form of the score function $\nabla_{\mathbf{z}} \log q(\mathbf{z}; \alpha_t, \sigma_t)$. One common approach is to train a noise estimator $\hat{\epsilon}_{\theta}$ by minimizing the expected L_2 error for samples drawn from q_{data} (see [11; 35; 32]):

$$\mathbb{E}_{\mathbf{x} \sim p_{data}} \mathbb{E}_{\epsilon \sim \mathcal{N}(\mathbf{0}, \sigma_t^2 \mathbf{I})} \|\hat{\epsilon}_{\theta}(\alpha_t \mathbf{x} + \sigma_t \epsilon, t) - \epsilon\|_2^2, \quad (4)$$

where (α_t, σ_t) are from the forward process (1). The common practice in diffusion models is to utilize a neural network of U-Net architecture [27] to represent the noise estimator $\hat{\epsilon}_{\theta}$. With (4), the score function can then be represented in terms of $\hat{\epsilon}_{\theta}(\mathbf{z}_t; t)$ as (see also (229) of [15])

$$\nabla_{\mathbf{z}} \log q(\mathbf{z}_t; \alpha_t, \sigma_t) = \frac{-(\mathbf{z}_t - \alpha_t \mathbf{x})}{\sigma_t^2} = -\hat{\epsilon}_{\theta}(\mathbf{z}_t; t)/\sigma_t. \quad (5)$$

Alternatively, the score function can be represented in terms of an estimator for \mathbf{x} (see [15]). The functional form for the noise level (α_t, σ_t) also plays an important role in the sampling quality in practice. For example, the setup $(\alpha_t, \sigma_t) = (1, \sqrt{t})$ was studied in [35], which corresponds to constant-speed heat diffusion. The recent work [15] found that a simple form of $(\alpha_t, \sigma_t) = (1, t)$ works well in practice.

3 Bi-directional Integration Approximation (BDIA) for DDIM

In this section, we first review DDIM inversion and EDICT as an extension of DDIM inversion. We then present our BDIA technique to enable exact diffusion inversion.

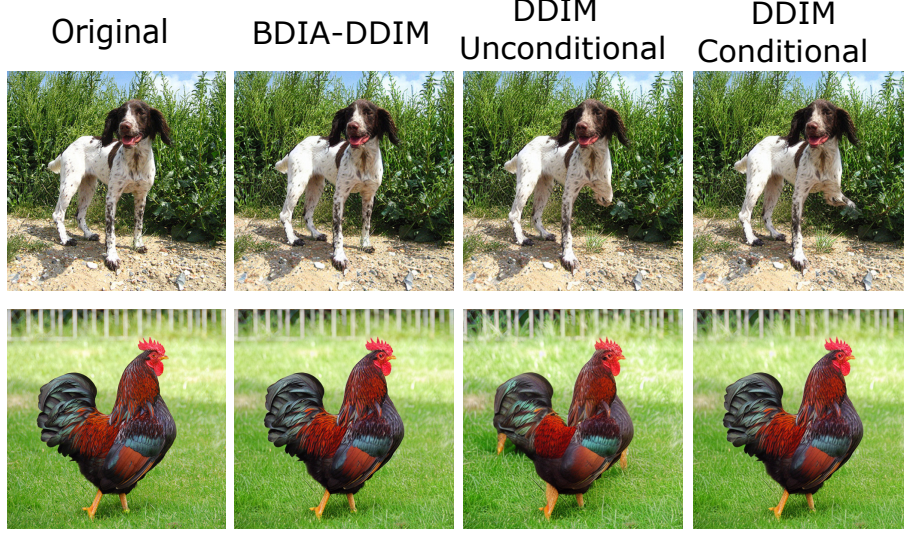


Figure 1: Demonstration of image reconstruction via BDIA-DDIM and DDIM. The total NFE for the round-trip (i.e., including both forward and backward iterations) DDIM procedure was 100 while the total NFE of BDIA-DDIM was set to 97 due to its special update formulation.

3.1 Review of DDIM inversion

We first consider the update expression of DDIM for sampling, which is in fact a first-order solver for the ODE formulation (2)-(3) (see [21; 40]), given by

$$\mathbf{z}_{i-1} = \alpha_{i-1} \left(\frac{\mathbf{z}_i - \sigma_i \hat{\boldsymbol{\epsilon}}_{\theta}(\mathbf{z}_i, i)}{\alpha_i} \right) + \sigma_{i-1} \hat{\boldsymbol{\epsilon}}_{\theta}(\mathbf{z}_i, i) \quad (6)$$

$$= a_i \mathbf{z}_i + b_i \hat{\boldsymbol{\epsilon}}_{\theta}(\mathbf{z}_i, i) \quad (7)$$

$$\approx \mathbf{z}_i + \int_{t_i}^{t_{i-1}} \mathbf{d}(\mathbf{z}_{\tau}, \tau) d\tau, \quad (8)$$

where $a_i = \alpha_{i-1}/\alpha_i$ and $b_i = \sigma_{i-1} - \sigma_i \alpha_{i-1}/\alpha_i$. It is clear from (6)-(8) that the integration $\int_{t_i}^{t_{i-1}} \mathbf{d}(\mathbf{z}_{\tau}, \tau) d\tau$ is approximated by the forward DDIM update. That is, only the diffusion state \mathbf{z}_i at the starting timestep t_i is used in the integration approximation.

To perform DDIM inversion, \mathbf{z}_i can be approximated in terms of \mathbf{z}_{i-1} as

$$\mathbf{z}_i = \alpha_i \left(\frac{\mathbf{z}_{i-1} - \sigma_{i-1} \hat{\boldsymbol{\epsilon}}_{\theta}(\mathbf{z}_i, i)}{\alpha_{i-1}} \right) + \sigma_i \hat{\boldsymbol{\epsilon}}_{\theta}(\mathbf{z}_i, i) \quad (9)$$

$$\approx \alpha_i \left(\frac{\mathbf{z}_{i-1} - \sigma_{i-1} \hat{\boldsymbol{\epsilon}}_{\theta}(\mathbf{z}_{i-1}, i)}{\alpha_{i-1}} \right) + \sigma_i \hat{\boldsymbol{\epsilon}}_{\theta}(\mathbf{z}_{i-1}, i), \quad (10)$$

where \mathbf{z}_i in the RHS of (9) is replaced with \mathbf{z}_{i-1} to facilitate explicit computation. This naturally introduces approximation errors, leading to inconsistency of the diffusion states between the forward and backward processes.

3.2 Review of EDICT for exact diffusion inversion

Inspired by the flow generative framework [17], the recent work [36] proposed EDICT to enforce exact diffusion inversion. The basic idea is to introduce an auxiliary diffusion state \mathbf{y}_i to be coupled with \mathbf{z}_i at every timestep i . The next pair of diffusion states $(\mathbf{z}_{i-1}, \mathbf{y}_{i-1})$ is then computed in an

alternating fashion as

$$\mathbf{z}_i^{\text{inter}} = a_i \mathbf{z}_i + b_i \epsilon_{\theta}(\mathbf{y}_i, i) \quad (11)$$

$$\mathbf{y}_i^{\text{inter}} = a_i \mathbf{y}_i + b_i \epsilon_{\theta}(\mathbf{z}_i^{\text{inter}}, i) \quad (12)$$

$$\mathbf{z}_{i-1} = p \mathbf{z}_i^{\text{inter}} + (1-p) \mathbf{y}_i^{\text{inter}} \quad (13)$$

$$\mathbf{y}_{i-1} = p \mathbf{y}_i^{\text{inter}} + (1-p) \mathbf{z}_{i-1}, \quad (14)$$

where $p \in [0, 1]$ is the weighting factor in the mixing operations and the pair $(\mathbf{z}_i^{\text{inter}}, \mathbf{y}_i^{\text{inter}})$ represents the intermediate diffusion states. According to [36], the two mixing operations (13)-(14) are introduced to make the update procedure stable.

Due to the alternating update formalism in (11)-(14), the computation can be inverted to obtain $(\mathbf{z}_i, \mathbf{y}_i)$ in terms of $(\mathbf{z}_{i-1}, \mathbf{y}_{i-1})$ as

$$\mathbf{y}_i^{\text{inter}} = (\mathbf{y}_{i-1} - (1-p)\mathbf{z}_{i-1})/p \quad (15)$$

$$\mathbf{z}_i^{\text{inter}} = (\mathbf{z}_{i-1} - (1-p)\mathbf{y}_i^{\text{inter}})/p \quad (16)$$

$$\mathbf{y}_i = (\mathbf{y}_i^{\text{inter}} - b_i \epsilon_{\theta}(\mathbf{z}_i^{\text{inter}}, i))/a_i \quad (17)$$

$$\mathbf{x}_i = (\mathbf{z}_i^{\text{inter}} - b_i \epsilon_{\theta}(\mathbf{y}_i, i))/a_i \quad (18)$$

Unlike (9)-(10), the inversion of (11)-(14) does not involve any approximation, thus enabling exact diffusion inversion.

Finally, it is clear from the above equations that the NFE that EDICT has to perform is two times the NFE required for DDIM. This makes the method computationally expensive in practice. It is highly desirable to reduce the NFE in EDICT while retaining exact diffusion inversion. We provide such a method in the next subsection.

3.3 BDIA-DDIM for exact diffusion inversion

Reformulation of DDIM update expression: In this section, we present our new technique BDIA to assist DDIM in achieving exact diffusion inversion. To do so, we first reformulate the update expression for \mathbf{z}_{i-1} in (7) in terms of all the historical diffusion states $\{\mathbf{z}_j\}_{j=N}^i$ as

$$\mathbf{z}_{i-1} = \mathbf{z}_N + \sum_{j=N}^i \Delta(t_j \rightarrow t_{j-1} | \mathbf{z}_j) \quad (19)$$

$$\approx \mathbf{z}_N + \sum_{j=N}^i \int_{t_j}^{t_{j-1}} \mathbf{d}(\mathbf{z}_{\tau}, \tau) d\tau, \quad (20)$$

where we use $\Delta(t_j \rightarrow t_{j-1} | \mathbf{z}_j)$ to denote approximation of the integration $\int_{t_j}^{t_{j-1}} \mathbf{d}(\mathbf{z}_{\tau}, \tau) d\tau$ via the forward DDIM step, given by

$$\begin{aligned} \Delta(t_j \rightarrow t_{j-1} | \mathbf{z}_j) &= \mathbf{z}_{j-1} - \mathbf{z}_j \\ &= a_j \mathbf{z}_j + b_j \hat{\epsilon}_{\theta}(\mathbf{z}_j, j) - \mathbf{z}_j. \end{aligned} \quad (21)$$

Replacing forward DDIM by backward DDIM: We argue that, in principle, the integration $\int_{t_j}^{t_{j-1}} \mathbf{d}(\mathbf{z}_{\tau}, \tau) d\tau$ in (20) can be alternatively approximated by the backward DDIM update, expressed as

$$\int_{t_j}^{t_{j-1}} \mathbf{d}(\mathbf{z}_{\tau}, \tau) d\tau \approx -\Delta(t_{j-1} \rightarrow t_j | \mathbf{z}_{j-1}), \quad (22)$$

where the notation $\Delta(t_{j-1} \rightarrow t_j | \mathbf{z}_{j-1})$ denotes the backward DDIM step from t_{j-1} to t_j . The minus sign in front of $\Delta(t_{j-1} \rightarrow t_j | \mathbf{z}_{j-1})$ is due to integration over reverse time. The update expression

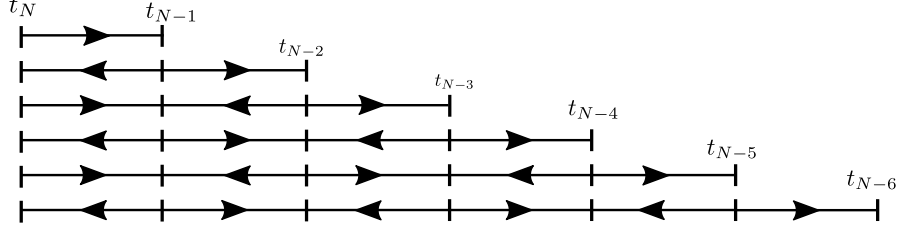


Figure 2: Schematic illustration of the BDIA-DDIM integration formulation. Right and left arrows denote forward and backward updates, respectively.

for the backward DDIM step can be represented as

$$\begin{aligned} \Delta(t_{j-1} \rightarrow t_j | \mathbf{z}_{j-1}) &= \mathbf{z}_j - \mathbf{z}_{j-1} \\ &= \alpha_j \left(\frac{\mathbf{z}_{j-1} - \sigma_{j-1} \hat{\mathbf{e}}_{\theta}(\mathbf{z}_{j-1}, j-1)}{\alpha_{j-1}} \right) + \sigma_j \hat{\mathbf{e}}_{\theta}(\mathbf{z}_{j-1}, j-1) - \mathbf{z}_{j-1} \end{aligned} \quad (23)$$

$$= \frac{\mathbf{z}_{j-1}}{a_j} - \frac{b_j}{a_j} \hat{\mathbf{e}}_{\theta}(\mathbf{z}_{j-1}, j-1) - \mathbf{z}_{j-1}. \quad (24)$$

It is noted that in practice, we first need to perform a forward DDIM step over $[t_j, t_{j-1}]$ to obtain \mathbf{z}_{j-1} , and then we are able to perform the backward DDIM step computing $\Delta(t_{j-1} \rightarrow t_j | \mathbf{z}_{j-1})$.

Bi-directional integration approximation (BDIA): We now present our new BDIA technique. Our primary goal is to develop an update expression for each \mathbf{z}_{i-1} as a linear combination of $(\mathbf{z}_{i+1}, \mathbf{z}_i, \hat{\mathbf{e}}_{\theta}(\mathbf{z}_i, i))$. As will be explained in the following, the summation of the integrations $\sum_{j=N}^i \int_{t_j}^{t_{j-1}} \mathbf{d}(\mathbf{z}_{\tau}, \tau) d\tau$ for \mathbf{z}_{i-1} will involve both forward DDIM updates and backward DDIM updates.

Suppose we are at the initial time step t_N with state \mathbf{z}_N . Then the next state \mathbf{z}_{N-1} is computed by applying the forward DDIM (see (21)):

$$\begin{aligned} \mathbf{z}_{N-1} &= a_N \mathbf{z}_N + b_N \hat{\mathbf{e}}_{\theta}(\mathbf{z}_N, N) \\ &= \mathbf{z}_N + \Delta(t_N \rightarrow t_{N-1} | \mathbf{z}_N). \end{aligned} \quad (25)$$

Upon obtaining \mathbf{z}_{N-1} , we are able to compute $\Delta(t_{N-1} \rightarrow t_N | \mathbf{z}_{N-1})$ over the previous time-slot $[t_{N-1}, t_N]$ and $\Delta(t_{N-1} \rightarrow t_{N-2} | \mathbf{z}_{N-1})$ over the next time-slot $[t_{N-1}, t_{N-2}]$. Consequently, the integration $\int_{t_N}^{t_{N-1}} \mathbf{d}(\mathbf{z}_{\tau}, \tau) d\tau$ can be approximated by $-\Delta(t_{N-1} \rightarrow t_N | \mathbf{z}_{N-1})$. We define the update for \mathbf{z}_{i-1} for $i \leq N-1$ as below:

Definition 1. When $i \leq N-1$, let the diffusion state \mathbf{z}_{i-1} be computed in terms of $(\mathbf{z}_i, \mathbf{z}_{i+1})$ as

$$\begin{aligned} \mathbf{z}_{i-1} &= \mathbf{z}_{i+1} + \left[a_i \mathbf{z}_i + b_i \hat{\mathbf{e}}_{\theta}(\mathbf{z}_i, i) \right] - \left(\frac{\mathbf{z}_i}{a_{i+1}} - \frac{b_{i+1}}{a_{i+1}} \hat{\mathbf{e}}_{\theta}(\mathbf{z}_i, i) \right) \\ &= \mathbf{z}_{i+1} - \Delta(t_i \rightarrow t_{i+1} | \mathbf{z}_i) + \Delta(t_i \rightarrow t_{i-1} | \mathbf{z}_i). \end{aligned} \quad (26)$$

We can conclude from (26) that in the computation of each \mathbf{z}_{i-1} , the integration for the most recent time-slot $[t_i, t_{i-1}]$ is approximated by a forward DDIM update, and the integration for the second most recent time-slot $[t_{i+1}, t_i]$ is approximated by a backward DDIM update. Fig. 2 demonstrates how the entire integration $\int_{t_N}^{t_{i-1}} \mathbf{d}(\mathbf{z}_{\tau}, \tau) d\tau$ for different \mathbf{z}_{i-1} is approximated. It can be seen from the figure that the directions of the integration approximation for neighbouring time-slots are always opposite. In other words, the forward and backward DDIM updates are interlaced over the set of time-slots $\{(t_j, t_{j-1})\}_{j=N}^i$ for each \mathbf{z}_{i-1} . We summarize the results in a proposition below:

Proposition 1. Let \mathbf{z}_{N-1} and $\{\mathbf{z}_i | i \leq N-2\}$ be computed by following (25) and (26) sequentially. Then for each timestep $i \leq N-2$, \mathbf{z}_i can be represented in the form of

$$\begin{aligned} \mathbf{z}_i &= \mathbf{z}_N + \Delta(t_N - t_{N-1} | \mathbf{z}_N) \bmod(N-j, 2) \\ &\quad + \sum_{j=i+1}^{N-1} (-\Delta(t_j \rightarrow t_{j+1} | \mathbf{z}_j) + \Delta(t_j \rightarrow t_{j-1} | \mathbf{z}_j)) \bmod(j-i, 2). \end{aligned} \quad (27)$$

BDIA-DDIM inversion: Whereas the conventional DDIM inversion (10) requires the approximation $z_{i-1} \approx z_i$, which is only true in the limit of infinite steps, the formulation (26) allows exact inversion (up to floating point error). Note that (26) is symmetric in time: switching the timestep t_{i+1} and t_{i-1} in (26) inverts the diffusion direction. That is, it follows from (26) that the diffusion state z_{i+1} can be computed in terms of (z_i, z_{i-1}) as

$$\begin{aligned} z_{i+1} &= z_{i-1} + \Delta(t_i \rightarrow t_{i+1}|z_i) - \Delta(t_i \rightarrow t_{i-1}|z_i) \\ &= z_{i-1} - \left[a_i z_i + b_i \hat{\epsilon}_\theta(z_i, i) \right] + \left(\frac{z_i}{a_{i+1}} - \frac{b_{i+1}}{a_{i+1}} \hat{\epsilon}_\theta(z_i, i) \right). \end{aligned} \quad (28)$$

We summarize the above property of time-symmetry in a lemma below:

Lemma 1 (time-symmetry). *Switching the timestep t_{i-1} and t_{i+1} in (26) produces the reverse update (28), and vice versa.*

Finally, similarly to the computation (28), EDICT also does not involve any approximation and results in exact diffusion inversion. However, in contrast to EDICT, (28) does not require a doubling of the NFE.

4 Related Works

In the literature, there is a branch of research on development of time-reversible ODE solvers. For instance, Verlet integration was a time-reversible method for solving 2nd-order ODEs [37]. Leapfrog integration is another time-reversible method also developed for solving 2nd-order ODEs [38].

5 Experiments

We conducted two types of experiments: (1) evaluation of image sampling for both BDIA-DDIM and BDIA-EDM; (2) image-editing via BDIA-DDIM. It was found that our new technique BDIA produces promising results for both tasks.

5.1 Evaluation of image sampling

In the first experiment, we consider the task of image sampling. The tested pre-trained models can be found in Appendix B. Given a pre-trained model, 50K artificial images were generated for a particular NFE, and the corresponding FID score was computed.

Table 1 and 2 summarize the computed FID scores. It is clear that by incorporating BDIA into both DDIM and EDM, the FID scores are improved. This can be explained by the fact that BDIA introduces the additional backward integration approximation per time-step in the sampling process. This makes the resulting final integration approximation become more accurate.

Table 1: Comparison of DDIM and BDIA-DDIM over CIFAR10

sampling methods	DDIM	BDIA-DDIM
NFE of 10	14.38	11.14

Table 2: Comparison of EDM and BDIA-EDM over CIFAR10

sampling methods	EDM	BDIA-EDM
NFE of 35	1.85	1.79

5.2 Evaluation of image-editing

In this second experiment, we evaluated BDIA-DDIM for image-editing by utilizing the open-source repository of EDICT¹. Fig. 3 visualizes the obtained results. We point out that BDIA-DDIM produces very similar results to EDICT while reducing by approximately half the NFE compared to EDICT.

¹<https://github.com/salesforce/EDICT>

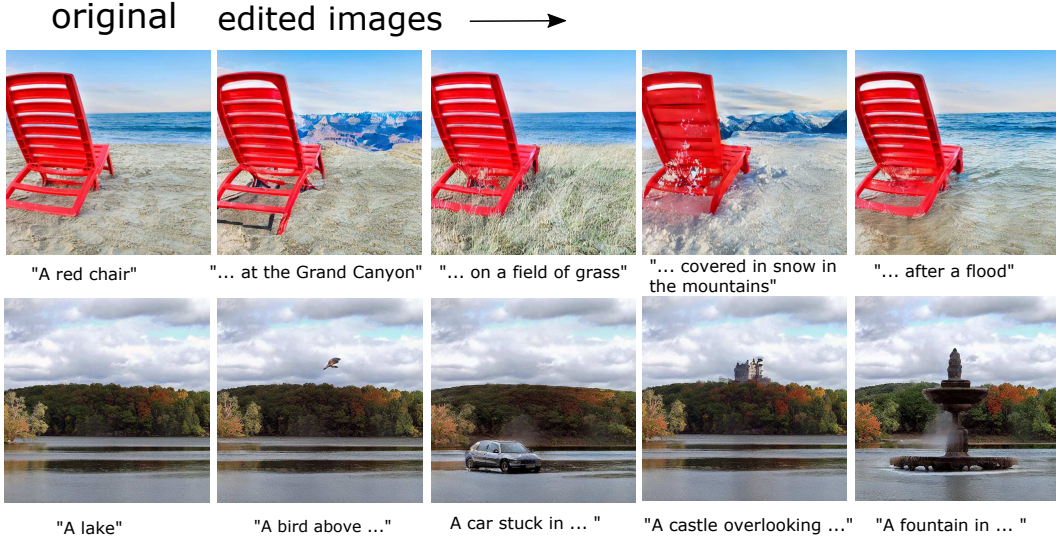


Figure 3: Image editing via BDIA-DDIM.

6 Conclusions

In this paper, we have proposed a new technique BDIA, to assist DDIM in achieving exact diffusion inversion. The key step of BDIA-DDIM is to perform DDIM update procedure twice at each time step t_i : one over the previous time-slot $[t_i, t_{i+1}]$ and the other over next time-slot $[t_i, t_{i-1}]$ in computing z_{i-1} . By doing so, the expression for z_{i-1} becomes a linear combination of $(z_i, \hat{e}_\theta(z_i, i), z_{i+1})$ that is symmetric in time. As a result, z_{i+1} can be computed exactly as a linear function of $(z_i, \hat{e}_\theta(z_i, i), z_{i-1})$, enabling exact diffusion inversion. Note that although the DDIM update is evaluated twice at each step, this is inexpensive since the costly neural functional evaluation is performed only once.

References

- [1] M. Arjovsky, S. Chintala, and L. Bottou. Wasserstein GAN. arXiv:1701.07875 [stat.ML], 2017.
- [2] F. Bao, C. Li, J. Sun, J. Zhu, and B. Zhang. Estimating the Optimal Covariance with Imperfect Mean in Diffusion Probabilistic Models. In *ICML*, 2022.
- [3] F. Bao, C. Li, J. Zhu, and B. Zhang. Analytic-DPM: an Analytic Estimate of the Optimal Reverse Variance in Diffusion Probabilistic Models. In *ICLR*, 2022.
- [4] C. M. Bishop. *Pattern Recognition and Machine Learning*. Springer, 2006.
- [5] N. Chen, Y. Zhang, H. Zen, R. J. Weiss, M. Norouzi, and W. Chan. WaveGrad: Estimating Gradients for Waveform Generation. arXiv:2009.00713, September 2020.
- [6] P. Dhariwal and A. Nichol. Diffusion models beat gans on image synthesis. arXiv:2105.05233 [cs.LG], 2021.
- [7] L. Dinh, D. Krueger, and Y. Bengio. Nice: Non-linear independent components estimation. arXiv preprint arXiv:1410.8516, 2014.
- [8] L. Dinh, J. Sohl-Dickstein, and S. Bengio. Density estimation using real nvp. arXiv preprint arXiv:1605.08803, 2016.
- [9] I. Goodfellow, J. Pouget-Abadie, M. Mirza, B. Xu, D. Warde-Farley, S. Ozair, A. Courville, and Y. Bengio. Generative Adversarial Nets. In *Proceedings of the International Conference on Neural Information Processing Systems*, pages 2672–2680, 2014.

- [10] I. Gulrajani, F. Ahmed, M. Arjovsky, V. Dumoulin, and A. C. Courville. Improved training of wasserstein gans. In *Advances in neural information processing systems*, pages 5767–5777, 2017.
- [11] J. Ho, A. Jain, and P. Abbeel. Denoising diffusion probabilistic models. In *NeurIPS*, 2020.
- [12] J. Ho and T. Salimans. Classifier-free diffusion guidance. arXiv preprint arXiv:2207.12598, 2022.
- [13] I. Huberman-Spiegelglas, V. Kulikov, and T. Michaeli. An Edit Friendly DDPM Noise Space: Inversion and Manipulations. arXiv:2304.06140v2 [cs.CV], 2023.
- [14] A. Hyvarinen. Estimation of non-normalized statistical models by score matching. *Journal of Machine Learning Research*, 24:695–709, 2005.
- [15] T. Karras, M. Aittala, T. Alia, and S. Laine. Elucidating the Design Space of Diffusion-Based Generative Models. In *36th Conference on Neural Information Processing Systems (NeurIPS)*, 2022.
- [16] D. Kim, Y. Kim, S. J. Kwon, W. Kang, and I.-C. Moon. Refining Generative Process with Discriminator Guidance in Score-based Diffusion Models. arXiv preprint arXiv:2211.17091 [cs.CV], 2022.
- [17] D. P. Kingma and P. Dhariwal. Glow: Generative flow with invertible 1x1 convolutions. In *Advances in neural information processing systems*, 2018.
- [18] D. P. Kingma, T. Salimans, B. Poole, and J. Ho. Variational diffusion models. arXiv: preprint arXiv:2107.00630, 2021.
- [19] M. W. Y. Lam, J. Wang, D. Su, and D. Yu. BDDM: Bilateral Denoising Diffusion Models for Fast and High-Quality Speech Synthesis. In *ICLR*, 2022.
- [20] L. Liu, Y. Ren, Z. Lin, and Z. Zhao. Pseudo Numerical Methods for Diffusion Models on Manifolds. In *ICLR*, 2022.
- [21] C. Lu, Y. Zhou, F. Bao, J. Chen, C. Li, and J. Zhu. DPM-Solver: A Fast ODE Solver for Diffusion Probabilistic Sampling in Around 10 Steps. In *NeurIPS*, 2022.
- [22] R. Mokady, A. Hertz, K. Aberman, Y. Pritch, and D. Cohen-Or. Null-text Inversion for Editing Real Images using Guided Diffusion Models. In *CVPR*, 2023.
- [23] A. Nichol and P. Dhariwal. Improved denoising diffusion probabilistic models. arXiv preprint arXiv:2102.09672, 2021.
- [24] A. Nichol, P. Dhariwal, A. Ramesh, P. Shyam, P. Mishkin, B. McGrew, I. Sutskever, and M. Chen. GLIDE: Towards Photorealistic image generation and editing with text-guided diffusion models. In *ICML*, 2022.
- [25] R. Rombach, A. Blattmann, D. Lorenz, P. Esser, and B. Ommer. High-resolution image synthesis with latent diffusion models. In *CVPR*, 2022.
- [26] R. Rombach, A. Blattmann, D. Lorenz, P. Esser, and B. Ommer. On High-resolution image synthesis with latent diffusion models. In *CVPR*, page 10684–10695, 2022.
- [27] O. Ronneberger, P. Fischer, and T. Brox. U-Net: Convolutional Networks for Biomedical Image Segmentation. arXiv:1505.04597 [cs.CV], 2015.
- [28] C. Saharia, W. Chan, S. Saxena, L. Li, J. Whang, E. Denton, S.-K.-S. Ghasemipour, B.-K. Ayan, S. S. Mahdavi, R.-G. Lopes, T. Salimans, J. Ho, D. J. Fleet, and M. Norouzi. Photorealistic text-to-image diffusion models with deep language understanding. arXiv preprint arXiv:2205.11487, 2022.
- [29] A. Sauer, K. Schwarz, and A. Geiger. StyleGAN-XL: Scaling StyleGAN to large diverse datasets. In *SIGGRAPH*, 2022.

- [30] Y. Shi, C. Xue, J. Pan, and W. Zhang. DragDiffusion: Harnessing Diffusion Models for Interactive Point-based Image Editing. arXiv:2306.14435v2, 2023.
- [31] J. Sohl-Dickstein, E. Weiss, N. Maheswaranathan, and S. Ganguli. Deep unsupervised learning using nonequilibrium thermodynamics. ICML, 2015.
- [32] J. Song, C. Meng, and S. Ermon. Denoising Diffusion Implicit Models. In *ICLR*, 2021.
- [33] Y. Song, C. Durkan, I. Murray, and S. Ermon. Maximum likelihood training of score-based diffusion models. In *Advances in neural information processing systems (NeurIPS)*, 2021.
- [34] Y. Song and S. Ermon. Generative modeling by estimating gradients of the data distribution. In *Advances in neural information processing systems (NeurIPS)*, page 11895–11907, 2019.
- [35] Y. Song, J. S.-Dickstein, D. P. Kingma, A. Kumar, S. Ermon, and B. Poole. Score-Based Generative Modeling Through Stochastic Differential Equations. In *ICLR*, 2021.
- [36] B. Wallace, A. Gokul, and N. Naik. EDICT: Exact Diffusion Inversion via Coupled Transformations. In *CVPR*, 2023.
- [37] L. Verlet. Computer Experiments on Classical Fluids. I. Thermodynamical Properties of Lennard-Jones Molecules. *Physical Review*, 159:98–103, 1967.
- [38] R. D. Skeel. Variable Step Size Destabilizes the Stamer/Leapfrog/Verlet Method. *BIT Numerical Mathematics*, 33:172–175, 1993.
- [39] G. Zhang, K. Niwa, and W. B. Kleijn. On Accelerating Diffusion-Based Sampling Processes by Improved Integration Approximation. arXiv:2304.11328 [cs.LG], 2023.
- [40] Q. Zhang and Y. Chenu. Fast Sampling of Diffusion Models with Exponential Integrator. arXiv:2204.13902 [cs.LG], 2022.

A Extension of the update procedure of (26)

As an extension of (26), we can also compute z_{i-1} by the update below:

Definition 2. When $i \leq N - 1$, let the diffusion state z_{i-1} be computed in terms of (z_i, z_{i+1}) as

$$\begin{aligned} z_{i-1} &= \gamma(z_{i+1} - z_i) + \left[a_i z_i + b_i \hat{\epsilon}_\theta(z_i, i) \right] - \gamma \left(\frac{z_i}{a_{i+1}} - \frac{b_{i+1}}{a_{i+1}} \hat{\epsilon}_\theta(z_i, i) - z_i \right) \\ &= z_i + \gamma(z_{i+1} - z_i) - \gamma \Delta(t_i \rightarrow t_{i+1} | z_i) + \Delta(t_i \rightarrow t_{i-1} | z_i), \end{aligned} \quad (29)$$

where $\gamma \in [0, 1]$.

B Tested Pre-trained Models for BDIA-DDIM and BDIA-EDM

Table 3: Tested pre-trained models in Table 1 and Table 2

BDIA-DDIM	ddim_cifar10.ckpt from https://github.com/luping-liu/PNDM
BDIA-EDM	edm-cifar10-32x32-cond-vp.pkl from https://github.com/NVlabs/edm